academicJournals

Vol. 12(13), pp. 146-162, 16 July, 2017
DOI: 10.5897/IJPS2017.4631
Article Number: 147138165272
ISSN 1992 - 1950

http://www.academicjournals.org/IJPS

International Journal of Physical Sciences

Full Length Research Paper

Estimation of depth to magnetic source bodies of Nsukka and Udi areas using spectral analysis approach

Gladys Ujunwa Edeh, Johnson Uchenna Abangwu, Agatha Ngozi Okwesili, Mirianrita Ngozi Ossai and Daniel Nnaemeka Obiora*

Department of Physics and Astronomy, University of Nigeria, Nsukka, Enugu State, Nigeria.

Received 18 April, 2017; Accepted 5 July, 2017

The study was aimed at estimating the depth to magnetic source bodies in Nsukka and Udi areas which falls within the Anambra basin. Aeromagnetic data were used and Spectral Analysis approach was employed in the quantitative interpretation. The total magnetic intensity (TMI) contour map which ranges from -53.1 to 133.7 nanoTesla (nT) was separated into regional and residual contour maps to produce a residual aeromagnetic intensity contour map. The residual intensity varies from -51.2 to 59.6 nT while the regional intensity varies from -8.7 to 85.1 nT. Depth results obtained from spectral analysis revealed two depth sources; the shallower magnetic source bodies and the deeper magnetic source bodies. The depth of shallower magnetic sources ranges from 314.12 to 1061.05 m with an average depth value of 632.32 m, whereas the depth of deeper magnetic sources vary from 1465.90 to 5888.73 m with an average depth value of 3260.41 m.

Key words: Magnetic source bodies, depth estimation, spectral analysis, Nsukka and Udi areas, aeromagnetic data

INTRODUCTION

Geophysical survey employing aeromagnetic method has become an essential and powerful tool for subsurface reconnaissance since it allows fast coverage of large areas and low cost per unit area explored, when compared with other geophysical methods. An aeromagnetic survey is a common type of geophysical survey carried out using a magnetometer aboard or towed behind an aircraft. The principle is similar to a magnetic survey carried out with a hand-held magnetometer, but allows much larger areas of the Earth's surface to be covered quickly for regional reconnaissance. The aircraft typically flies in a grid-like pattern with height and line spacing determining the resolution of the data (and cost of the survey per unit area). As the aircraft flies, the magnetometer records tiny variations in the intensity of the ambient magnetic field due to the temporal effects of the constantly varying solar wind and spatial variations in the Earth's magnetic field because of the regional magnetic field, and the local effect of magnetic minerals in the Earth's crust. The purpose of magnetic surveying is to identify and describe regions of the Earth's crust that have anomalous

*Corresponding author. E-mail: daniel.obiora@unn.edu.ng.

magnetizations. In the realm of applied geophysics, these anomalous magnetizations might be associated with local mineralization that is potentially of commercial interest, or they could be due to subsurface structures that have a bearing on the location of oil deposits.

No geophysical work on the determination of depth to magnetic source bodies has been carried out in Nsukka and Udi areas, though some work have been done in Anambra Basin in which the study area falls. Few geophysical studies have been reported in Nsukka area alone by Obiora et al. (2015) and Obiora et al. (2016) in which they investigated among other things, the depth to magnetic and gravity anomalous bodies and the possible mineralization in the area, through the interpretation of aeromagnetic and gravity data. Other geophysical works that have been carried out in Nsukka and Udi areas are mainly on hydrogeological investigations of groundwater potential and vulnerability (Ugwuanyi et al., 2015; Aleke et al., 2016).

Geology of the area

The study area lies between latitude 6° 00′ N – 7° 00′N and longitude 7° 00′E – 7° 30′E in Enugu State, southeastern Nigeria. It covers a total surface area of approximately 6050 square kilometers. The highest point in Nsukka area is about 590 m above datum level plane, but the lowlands generally have heights below 250 m above sea level, while the average elevation of Udi area is about 437 m. Nsukka and Udi area is a sedimentary Basin within the Anambra Basin underlain by rocks which range in age from Coniacian to Paleocene. The geology of the area is composed of Imo formation of Paleocene, Nsukka formation, Ajali formation of Maastrichtian and Mamu formation (Nwajide and Reijers, 1995; Onwuemesi, 1995). The Mamu formation is made up of fine medium grained white to grey sandstones, shaly sandstones, sandy shales, grey mudstones, shales and coal seams. This conformably underlies the Ajali formation. The Ajali formation consist of thick friable, poorly sorted sandstones, which is white in colour but sometimes iron stained. The Nsukka formation lies conformably on the Ajali sandstone and consists of an alternating succession of sandstone, dark shale and sandy shale, with thin coal seams at various horizons. Figure 1 shows the geologic map of Nsukka and Udi areas.

Source of data

Nsukka (sheet 287) and Udi (sheet 301) aeromagnetic data were gotten from the Nigerian Geological Survey Agency (NGSA). Furgo Airborne Surveys obtained the aeromagnetic data using a proton precession magnetometer at a flight altitude of 80 m, along NE-SW flight lines that were spaced at 500 m. The data were recorded in digitized form (X, Y, Z text file) after removing the geomagnetic gradient from the raw data using International Geomagnetic Reference Field (IGRF), 2009, with intensity of 33095 nT (nanoTesla), angles of inclination and declination of -13.279° and -1.449°, respectively. X and Y represent the longitude and latitude of Nsukka and Udi areas in meters, respectively, while Z represents the magnetic field intensity measured in nanoTesla.

METHODOLOGY

Procedure and data analysis

The procedures employed in this study include the following:

(a) Merging of the two sheets into one sheet and production of Total Magnetic Intensity (TMI) map of the study area using Oasis Montaj software.
(b) Application of gridding, polynomial fitting (regional and residual separation) and enhancement processes such as derivatives and upward continuation to the TMI grid using Oasis Montaj software.
(c) Spectral depth determination to magnetic source bodies.

A potential field measured on a given observation plane at a constant height can be recalculated as though the observations were made on a different plane, either higher (upward continuation) or lower (downward continuation). The upward continuation smoothen the anomalies obtained at the ground surface by projecting the surface mathematically upward above the original datum. Computation of the first vertical derivative in an aeromagnetic survey is equivalent to observing the vertical gradient directly with a magnetic gradiometer and has the advantages of enhancing shallow sources, suppressing deeper ones, and giving a better resolution of closely-spaced sources. Second, third and higher order vertical derivatives may also be computed to pursue this effect further, but usually the noise in the data becomes more prominent than the signal at above the second vertical derivative (Reeves, 2005). Horizontal derivatives may also be calculated, noting that a direction (azimuth) needs to be chosen, giving another element of choice for optimum presentation. Alternatively, the maximum horizontal gradient at each grid point can be displayed, regardless of direction.

Spectral analysis is a quantitative method, based on the properties of the energy spectrum of large and complex aeromagnetic data set. It uses the 2-D Fast Fourier Transform and transforms magnetic data from space domain to frequency domain. The major advantage of Spectral analysis method is its ability to filter almost all the noise from the data whilst still making sure no information is lost in the process of interpretation by overlapping data. Such techniques of spectral analysis provide rapid depth estimates from regularly-spaced digital field data. Bhattacharyya (1966), Spector and Grant (1970) and Shuey et al. (1977) described 2-D techniques for spectral analysis of aeromagnetic anomalies. An expression derived by Bhattacharyya (1966) for the power spectrum of the total magnetic field intensity over a single rectangular block was generalized by Spector and Grant (1970), by assuming that the anomalies on an aeromagnetic map are due to an ensemble of vertical prisms (Nwankwo et al., 2011). They showed that contributions from the depth, width and thickness of a magnetic source ensemble could affect the shape of the energy spectrum. The depth factor, however, is the dominant term that controls the shape. The power spectrum function is transformed mathematically by technique of Fourier and the logarithm of the power contained in each frequency of the field that the sources create at a distance h, decreases linearly with increasing frequency

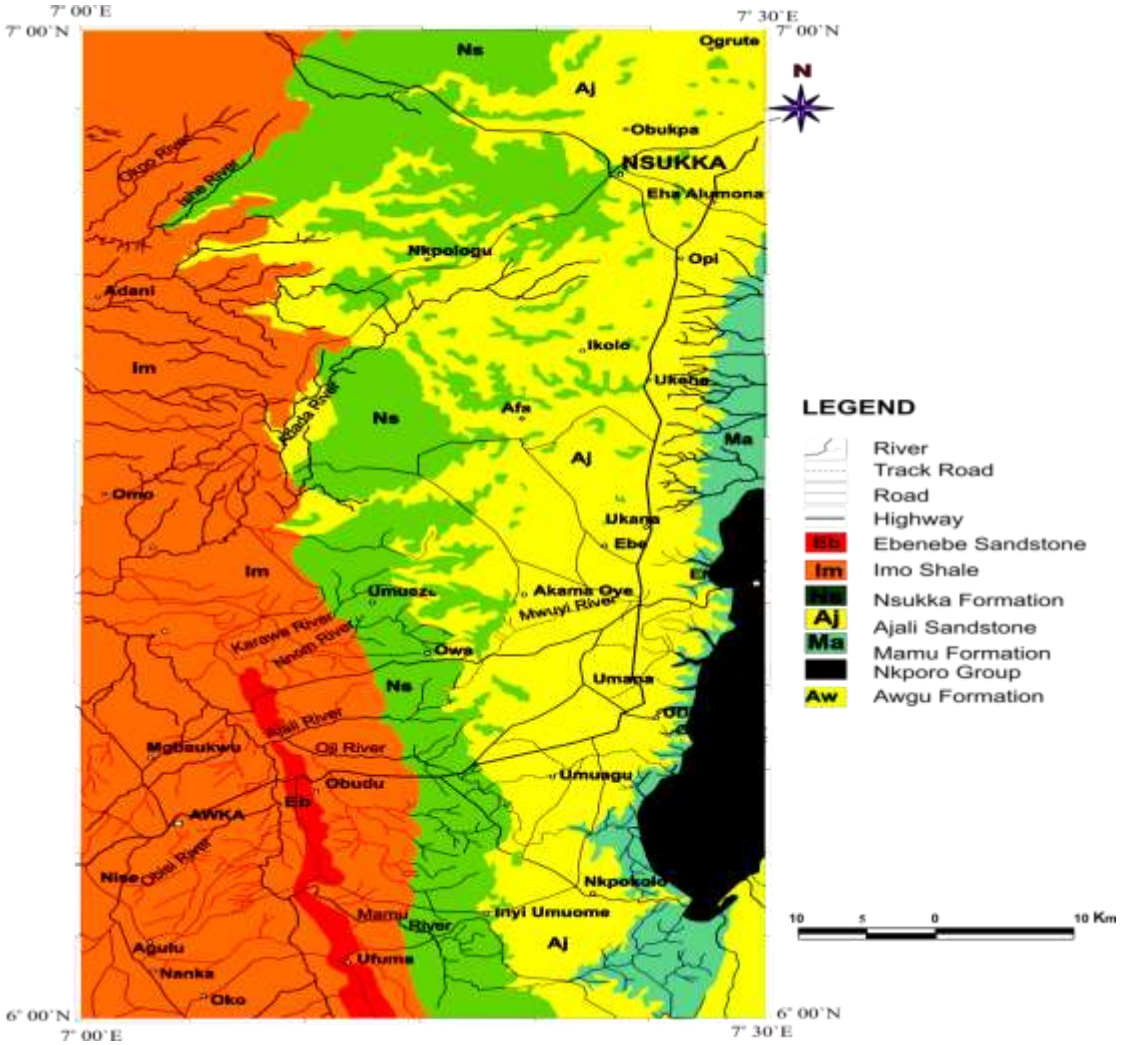

Figure 1. Geological map of Nsukka and Udi area.

within discrete segments of the spectrum (Tadjou et al., 2009). Estimation of depth to the top of magnetic sources follows directly from considering the power spectrum (PS) due to an ensemble of magnetic sources that are at an average depth (h) from the observation elevation given by

$$PS(k) = Ce^{-4\pi hf} = Ce^{-2hk} \quad (1)$$

where f is the frequency (= 1/λ, λ is the wavelength) in cycles/unit distance that corresponds to wavenumber, k = 2πf = 2π/λ in radians/unit distance, and C is a constant which includes field parameters and magnetic properties.

Taking the natural logarithm of both sides of Equation 1, expresses the power spectrum in the linear equation:

$$\ln[PS(k)] = \ln[C] - 4\pi hf = \ln[C] - 2hk \quad (2)$$

where ln[C] is the intercept and 4πh or 2h is the gradient of the straight line plot of the ln[P S] against f or k, respectively. Thus the average depth to magnetic sources is computed from the gradient as (Hinze et al., 2013):

$$h(f) = |\text{gradient}|/4\pi = |\text{gradient}| \times 0.08 \text{ cycles/unit distance} \quad (3a)$$

or

$$h(k) = |\text{gradient}|/2 = |\text{gradient}| \times 0.5 \text{ radians/unit distance} \quad (3b)$$

Graphs of the logarithms of the spectral energies against frequencies are plotted and linear segment from the low frequency part of the spectra representing contributions from the deep magnetic anomalies could be drawn from each graph. The gradient of the linear segment is evaluated and the depth to the magnetic bodies is calculated using (Spector and Grant, 1970; Hahn et al., 1976):

$$h = -\frac{M}{4\pi} \quad (4)$$

where $M = \frac{\log E}{f}$ is the gradient and $E(f) = e^{-2hf}$ is the energy spectrum and Log E is the variation of the logarithm of the power spectrum in the interval of frequency Δ (f). The energy

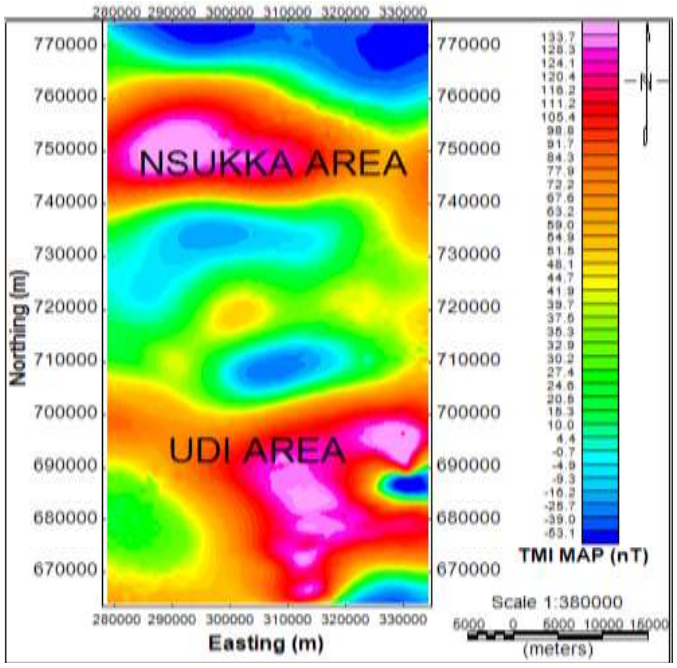

Figure 2. TMI map of the study area.

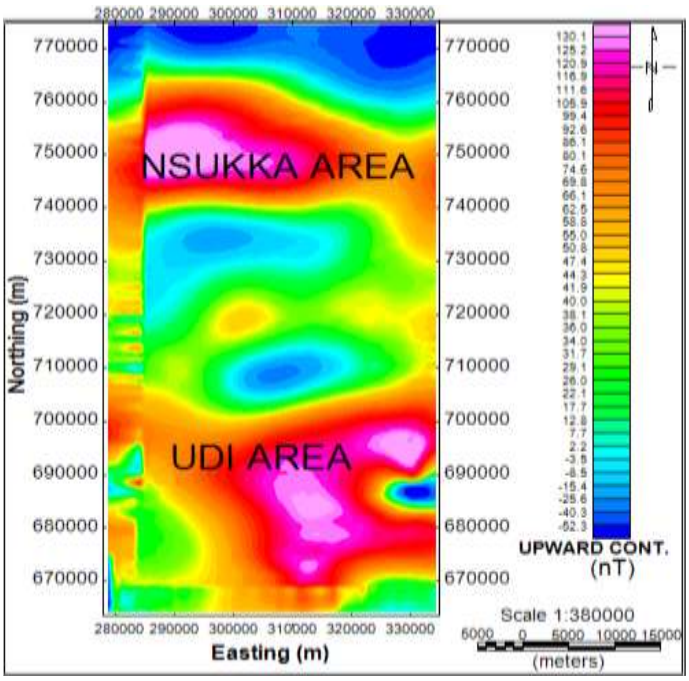

Figure 3. Upward continuation of the study area.

spectrum generally has two sources. The deeper source is manifested in the smaller wavenumber end of the spectrum, while the shallower ensemble manifests itself in the larger wavenumber end. The tail of the spectrum is a consequence of high wavenumber noise (Tadjou et al., 2009). The graph of Log E against Frequency is drawn for eighteen cells.

RESULTS

The total magnetic intensity (TMI) was produced into map which is in different colour aggregate and varies from -53.1 nT to 133.7 nT (Figure 2). Figure 3 shows the

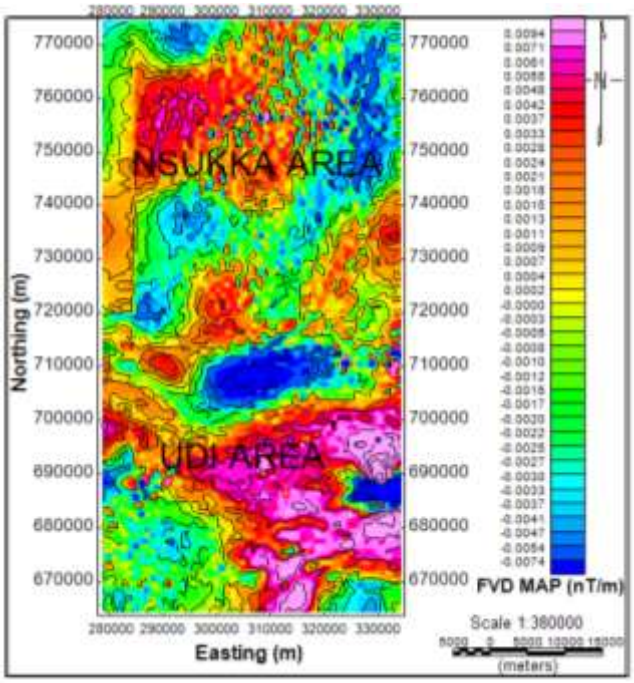

Figure 4. First vertical derivative map.

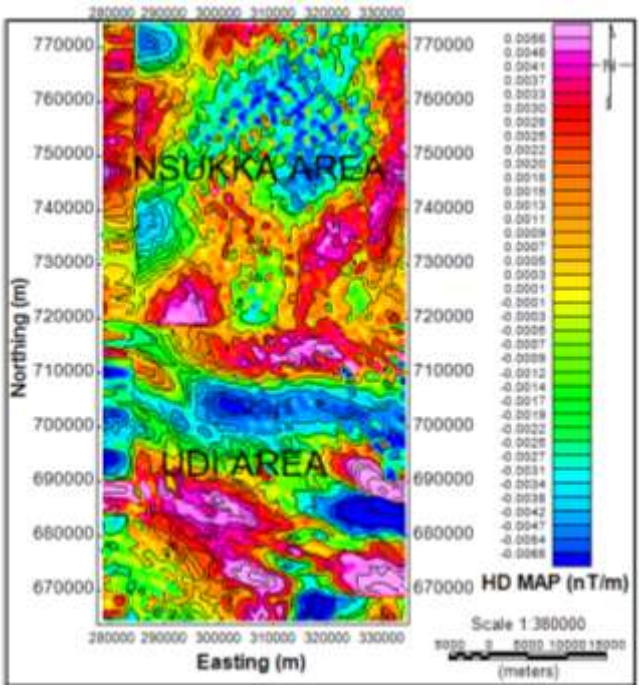

Figure 5. Horiontal derivative map.

upward continuation map of the study area with magnetic intensity varying from -52.3 to 130.1 nT. Random noise was removed by upward continuation of the aeromagnetic anomaly field to a height of 125 m before producing the upward continued aeromagnetic anomaly map of the sheet. Figures 4 and 5 show the first vertical derivative (FVD) and horizontal derivative (HD) maps of the study area, respectively. First vertical derivative

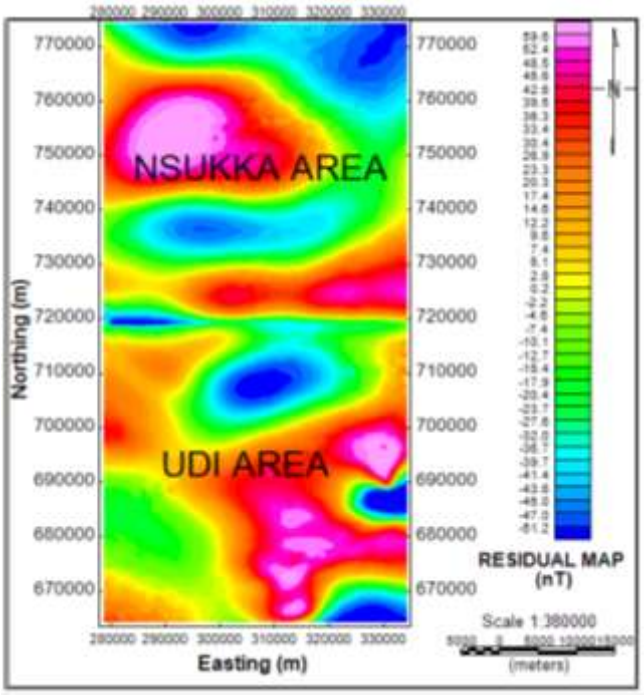

Figure 6. Residual map of the study area.

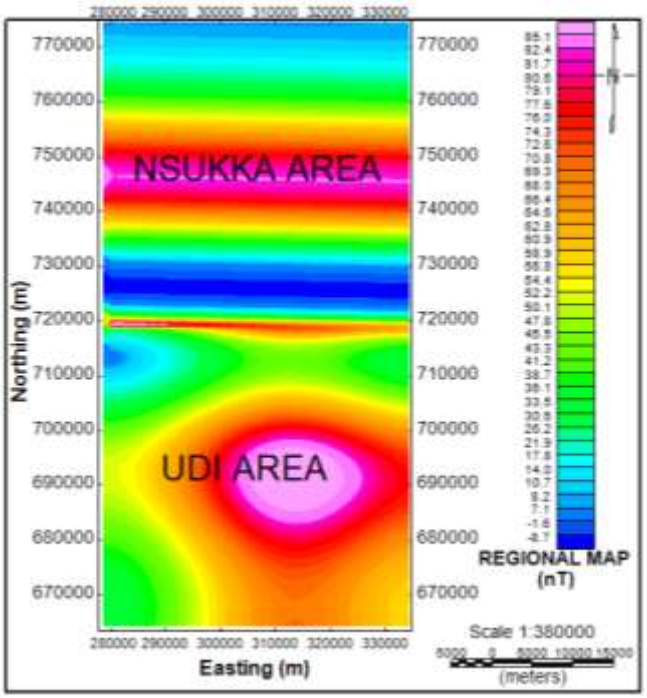

Figure 7. Regional map of the study area.

(FVD) enhanced shallow sources by suppressing deeper ones and gave a better resolution to closely spaced sources. The regional field ranging from -8.7 to 85.1 nT (Figure 7) was removed from the total magnetic intensity map to obtain the residual map (Figure 6) with a first order polynomial fitting. The magnetic intensity of the

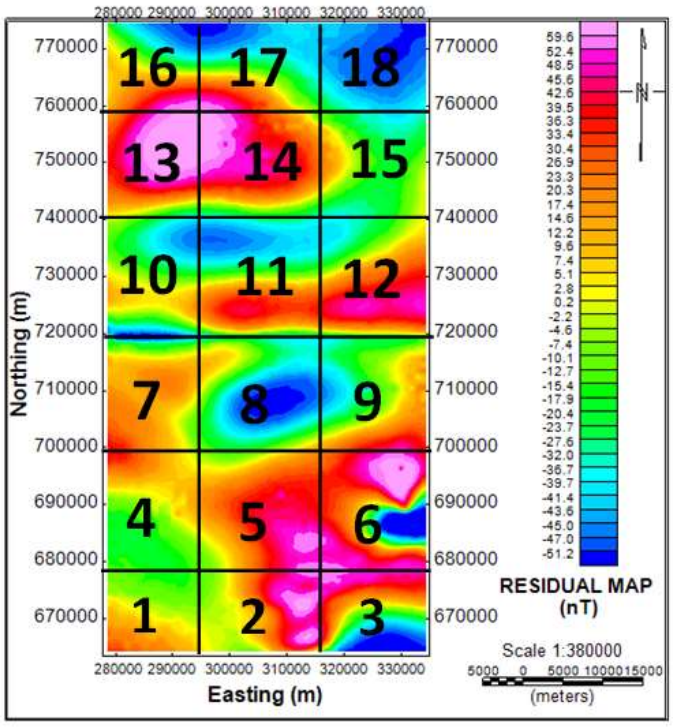

Figure 8. Map of spectral cell division.

residual map varies from -51.2 to 59.6 nT.

The magnetic residual map was subdivided into 18 spectral blocks (Figure 8) allowing spectral probe of 18.33 km by 18.33 km area, for the purpose of easy handling of the large surface area involved. A window that is too small will not capture sufficient anomalies for averaging and one that is too large will average the depths over too great a length or region to have geological meaning. Figure 9 shows the graph of log E against frequency for the eighteen spectral blocks. For each block, two linear segments could be identified which implies that there are two magnetic source layers in the study area; the deep and shallow magnetic sources. The gradients of the deep segment are represented by lines with red colour and the gradients of the shallow segments are represented by lines with blue colour.

From the plots shown in Figure 9, Equation 4 was used to calculate the depths of deep (Table 1) and shallow (Table 2) magnetic sources and the summarized result is shown in Table 3. From the computed values (Table 3), the magnetic basement depth map was plotted and contoured using surfer 10 software. The depth of the shallower magnetic sources (Table 2) varies from 314.12 m to 1061.05 m with an average depth of 632.32 m, whereas the depth of the deeper magnetic sources vary from 1465.90 to 5888.73 m with an average value of 3260.41 m. Figure 10 (a, b) show the 2D and 3D contour maps of the shallow depth of magnetic source anomalies, while Figure 11 (a, b) show the 2D and 3D contour maps of the deep depth of magnetic source bodies.

DISCUSSION

The TMI map (Figure 2) shows that the TMI anomaly values vary from –53.1 nT to 133.7 nT, while the residual values (Figure 6) are from –51.2 nT to 59.6 nT. Areas of low and high TMI values are revealed by the colour legend bar. The high amplitude anomalies were observed in the southeast and northwest parts of the study area, while the low amplitude anomalies were seen in the north central part of the area. The regional field ranges from -8.7 to 85.1 nT (Figure 7). The results from the spectral analysis (Table 3) show that the depth of the shallower magnetic sources vary from 314.12 to 1061.05 m with an average depth value of 632.32 m, whereas the depth of the deep magnetic sources vary from 1465.90 to 5888.73 m with an average depth value of 3260.41 m. Figures 10 and 11 which are contour maps of shallow and deep magnetic sources, respectively, were produced in colour aggregate as indicated by the legend. Locations with blue colour correspond to the deeper depth areas, while the places with dust colour depicted lowest depth to magnetic source bodies.

The depth results obtained from the present work is higher than the depth results obtained by Obiora et al. (2015), who worked on Nsukka area alone, though they did not employ spectral analysis. They got highest depth

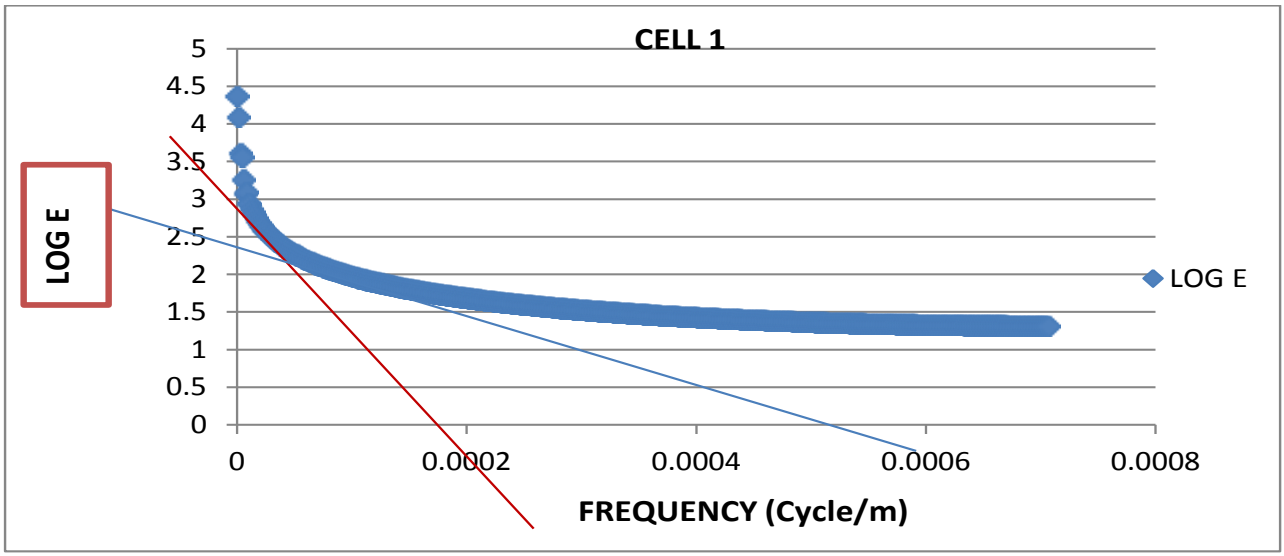
CELL 1
LOG E
5
4.5
4
3.5
3
2.5
2
1.5
1
0.5
0
0
0.0002
0.0004
0.0006
0.0008
FREQUENCY (Cycle/m)
LOG E

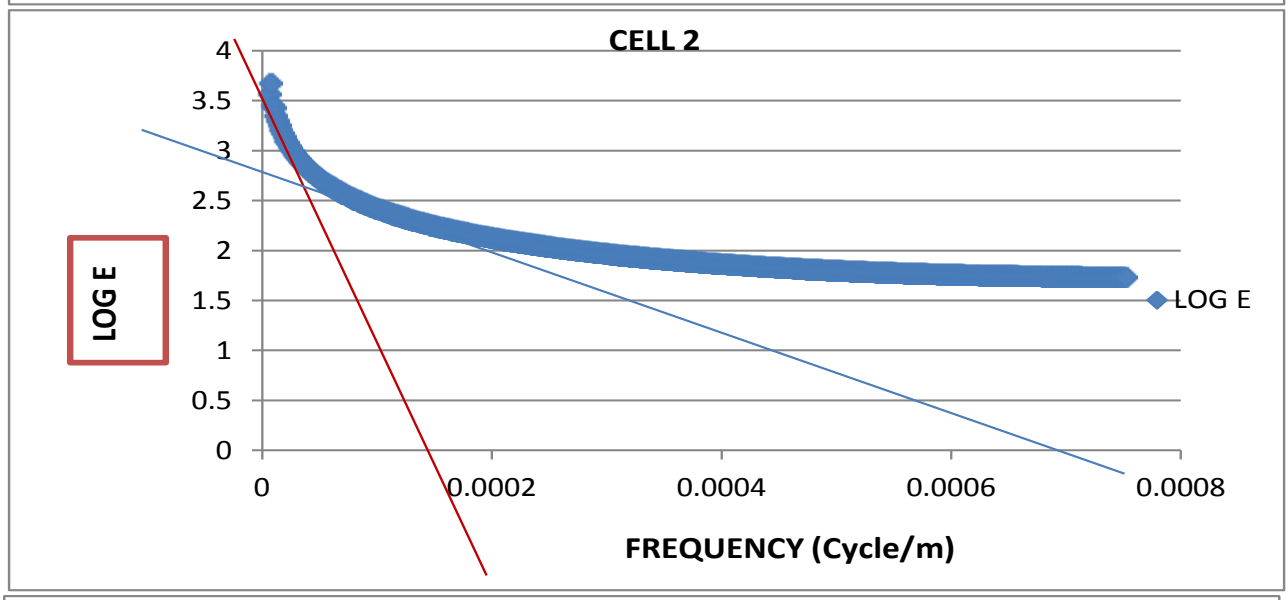
CELL 2
LOG E
4
3.5
3
2.5
2
1.5
1
0.5
0
0
0.0002
0.0004
0.0006
0.0008
FREQUENCY (Cycle/m)
LOG E

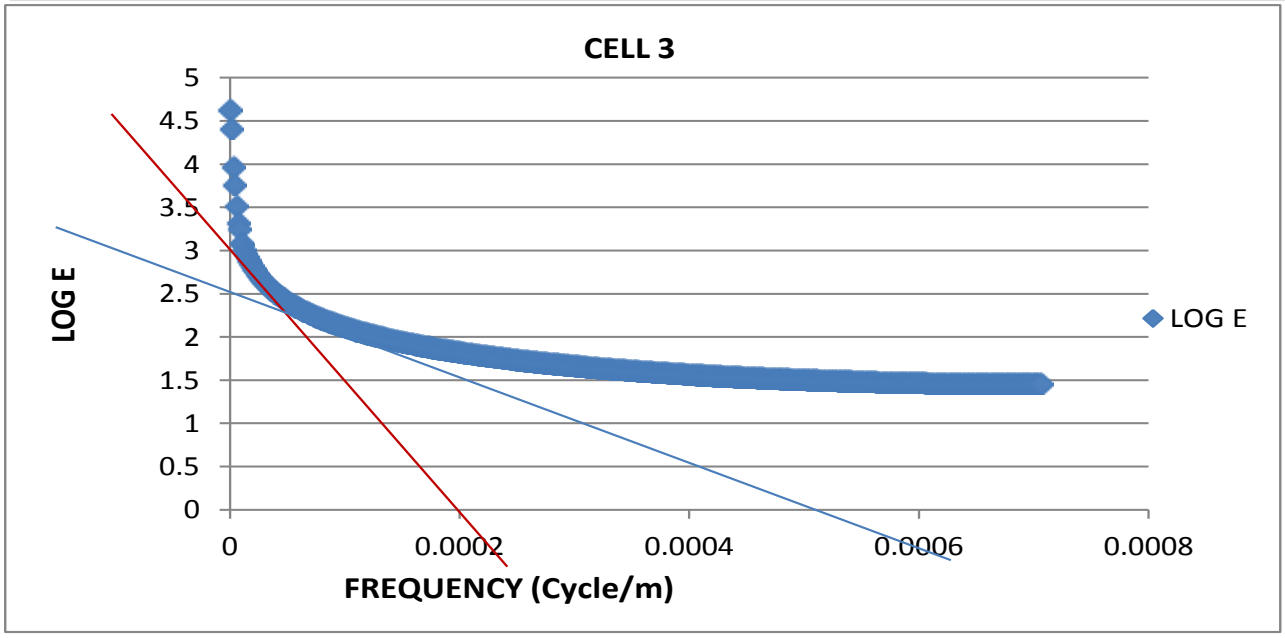
CELL 3
LOG E
5
4.5
4
3.5
3
2.5
2
1.5
1
0.5
0
0
0.0002
0.0004
0.0006
0.0008
FREQUENCY (Cycle/m)
LOG E

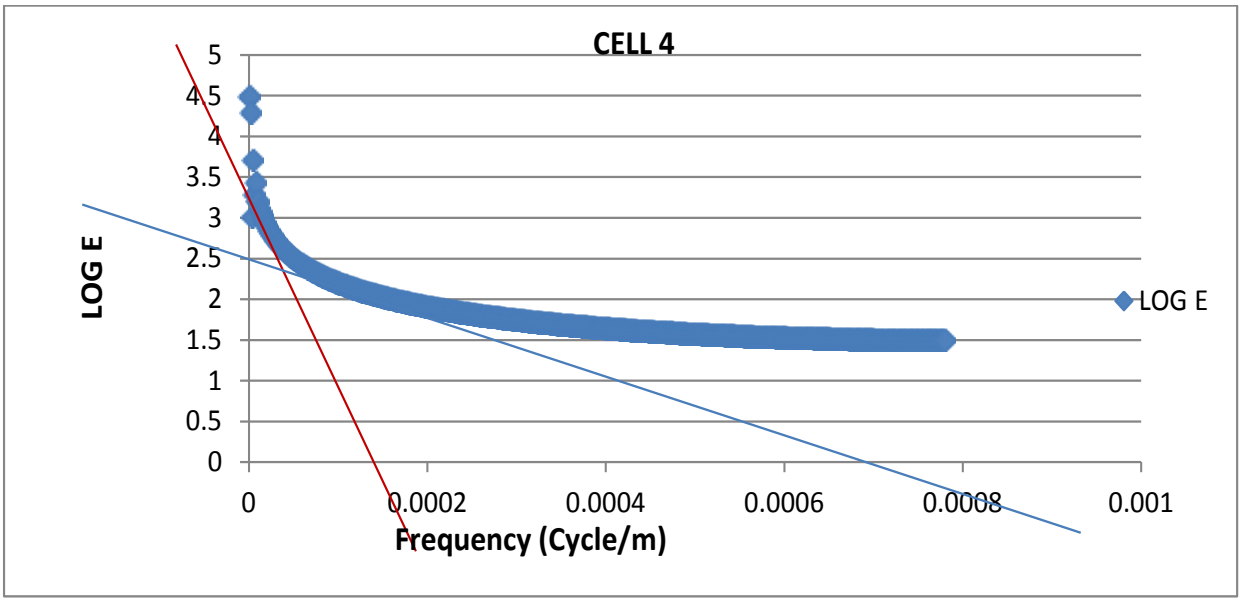
CELL 4
LOG E
Frequency (Cycle/m)
LOG E
0
0.5
1
1.5
2
2.5
3
3.5
4
4.5
5
0
0.0002
0.0004
0.0006
0.0008
0.001

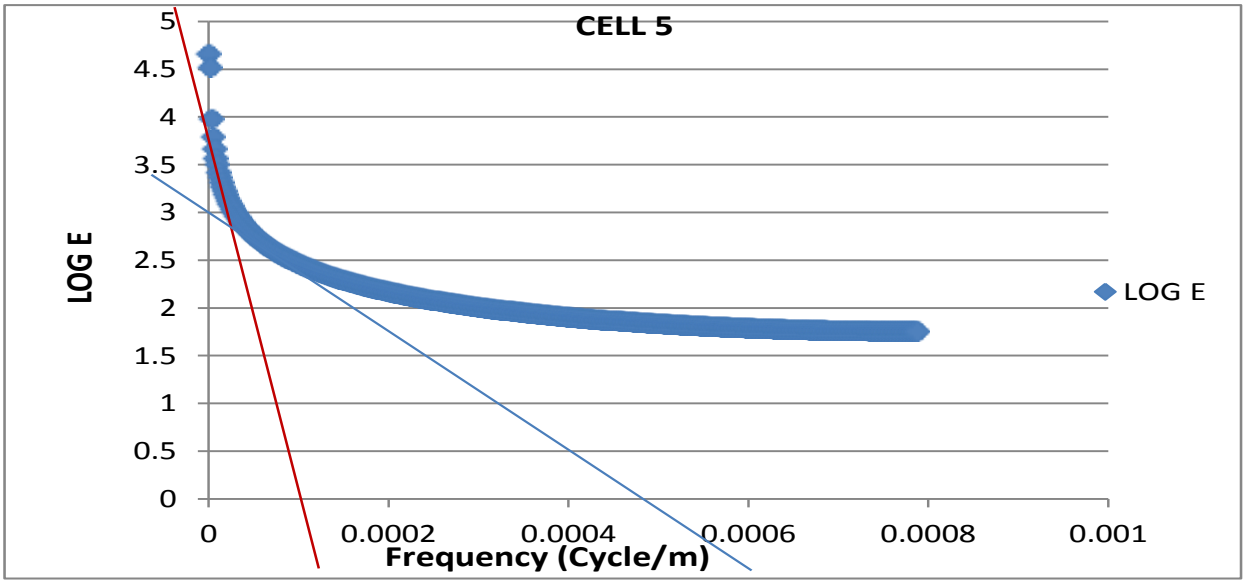
CELL 5
LOG E
Frequency (Cycle/m)
LOG E
0
0.5
1
1.5
2
2.5
3
3.5
4
4.5
5
0
0.0002
0.0004
0.0006
0.0008
0.001

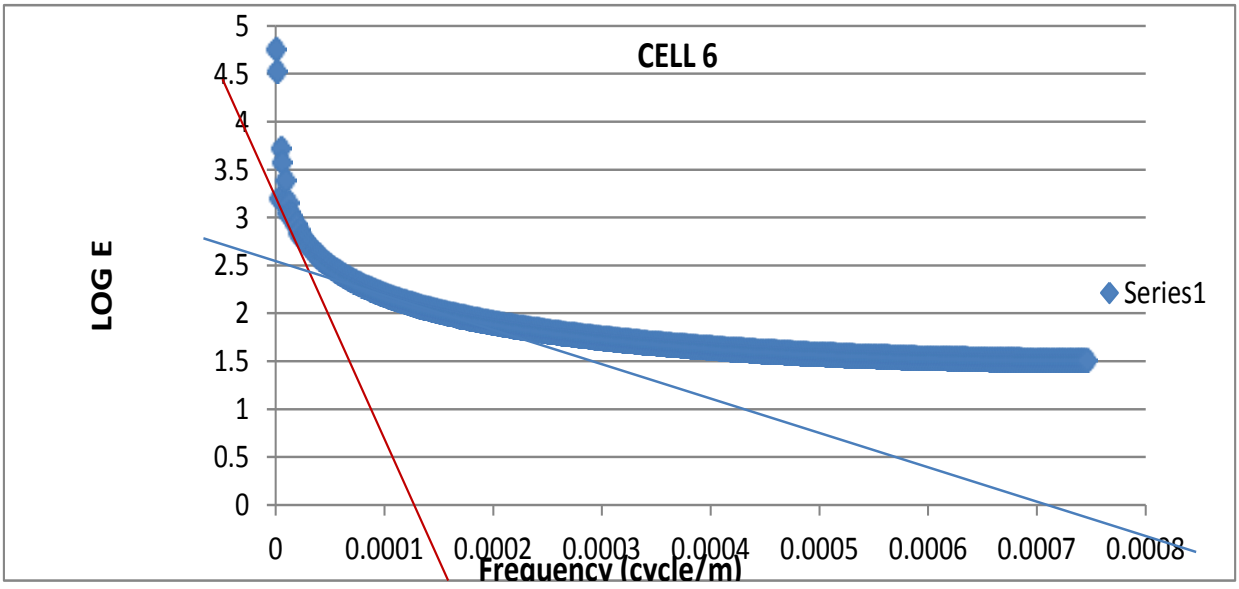
CELL 6
LOG E
Frequency (cycle/m)
Series1
0
0.5
1
1.5
2
2.5
3
3.5
4
4.5
5
0
0.0001
0.0002
0.0003
0.0004
0.0005
0.0006
0.0007
0.0008

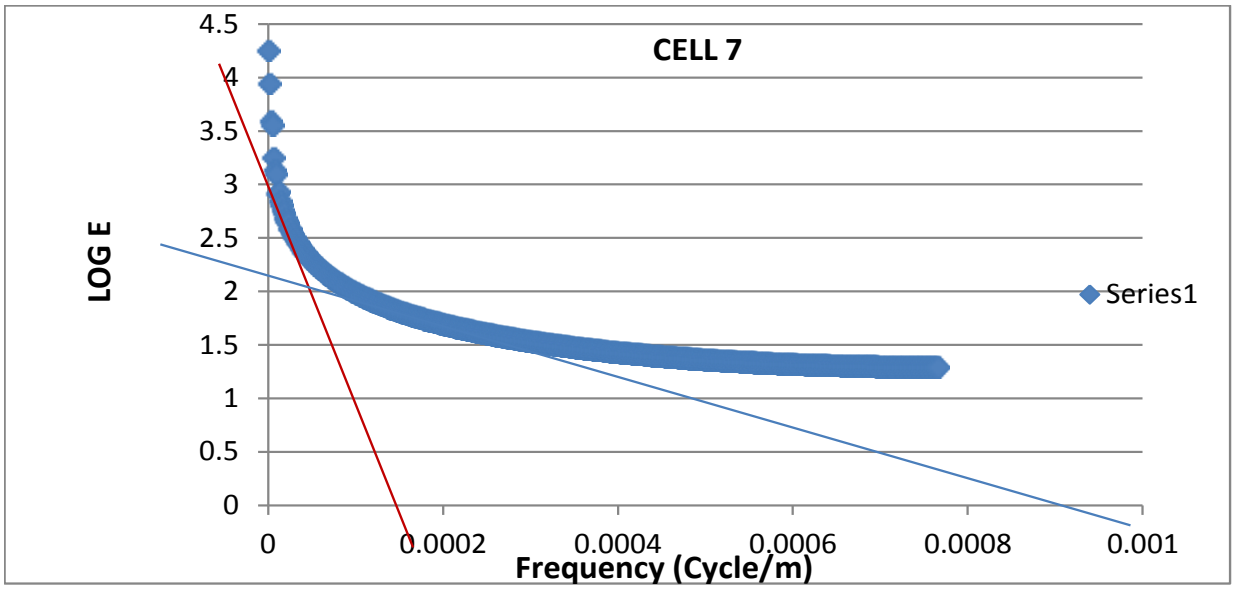
CELL 7
LOG E
4.5
4
3.5
3
2.5
2
1.5
1
0.5
0
0
0.0002
0.0004
0.0006
0.0008
0.001
Frequency (Cycle/m)
Series1

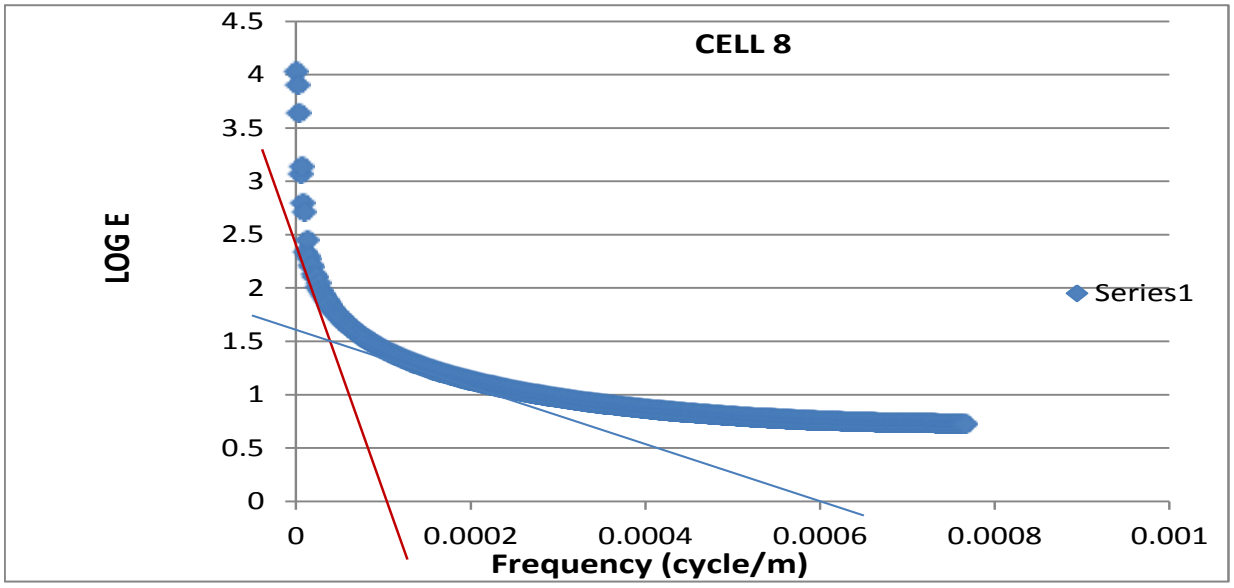
CELL 8
LOG E
4.5
4
3.5
3
2.5
2
1.5
1
0.5
0
0
0.0002
0.0004
0.0006
0.0008
0.001
Frequency (cycle/m)
Series1

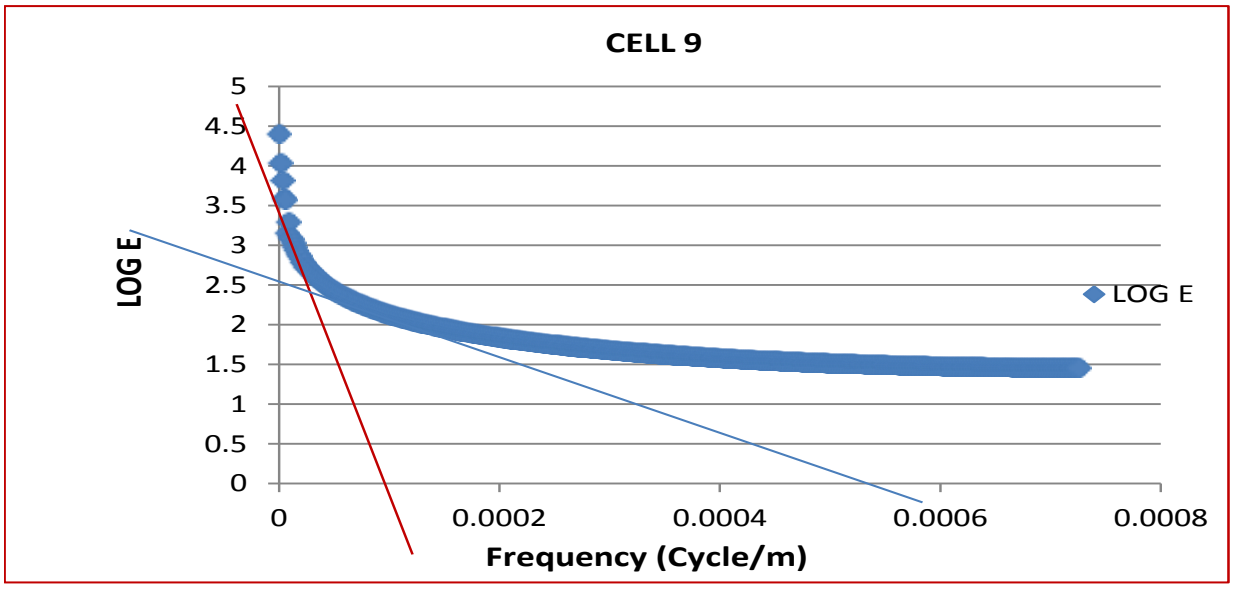
CELL 9
LOG E
5
4.5
4
3.5
3
2.5
2
1.5
1
0.5
0
0
0.0002
0.0004
0.0006
0.0008
Frequency (Cycle/m)
LOG E

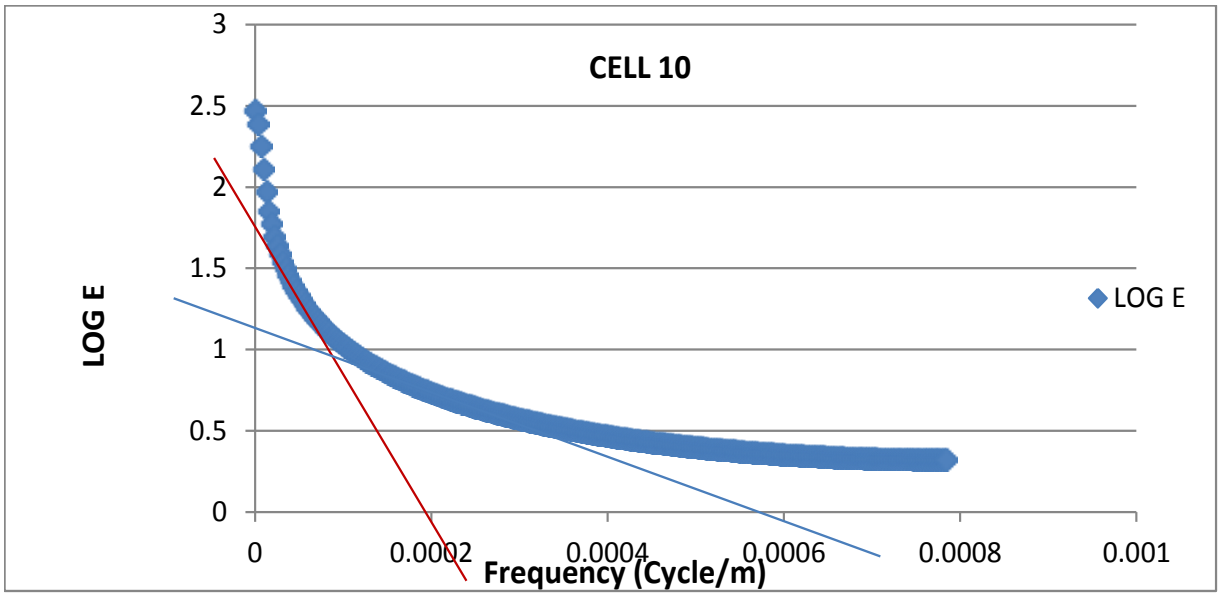
CELL 10
LOG E
Frequency (Cycle/m)
LOG E
3
2.5
2
1.5
1
0.5
0
0
0.0002
0.0004
0.0006
0.0008
0.001

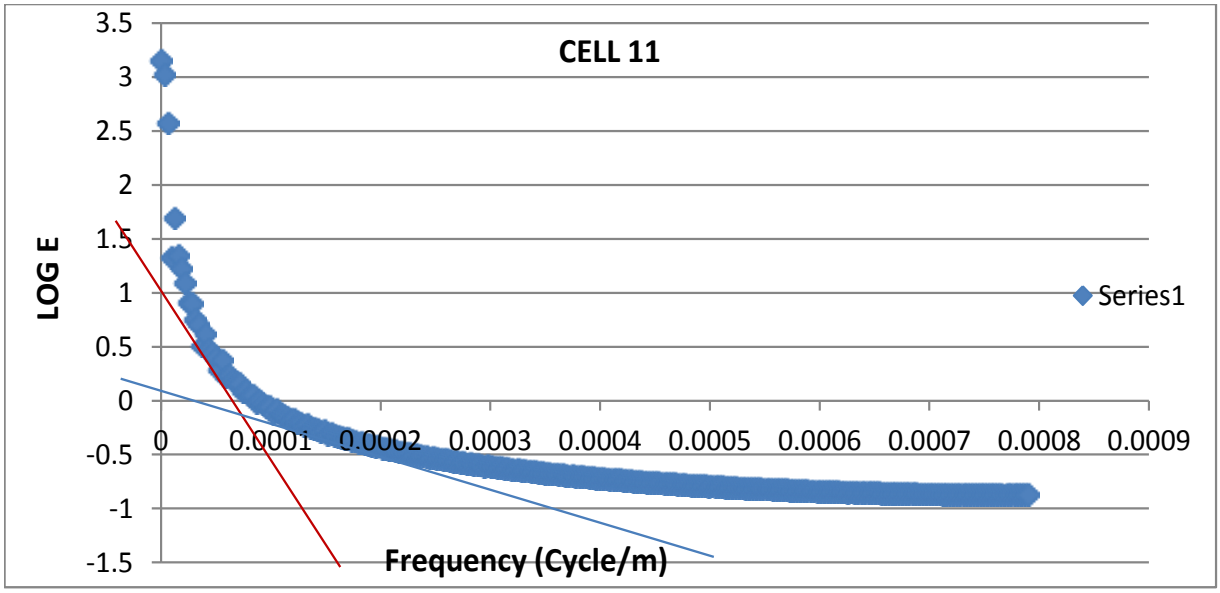
CELL 11
LOG E
Frequency (Cycle/m)
Series1
3.5
3
2.5
2
1.5
1
0.5
0
-0.5
-1
-1.5
0
0.0001
0.0002
0.0003
0.0004
0.0005
0.0006
0.0007
0.0008
0.0009

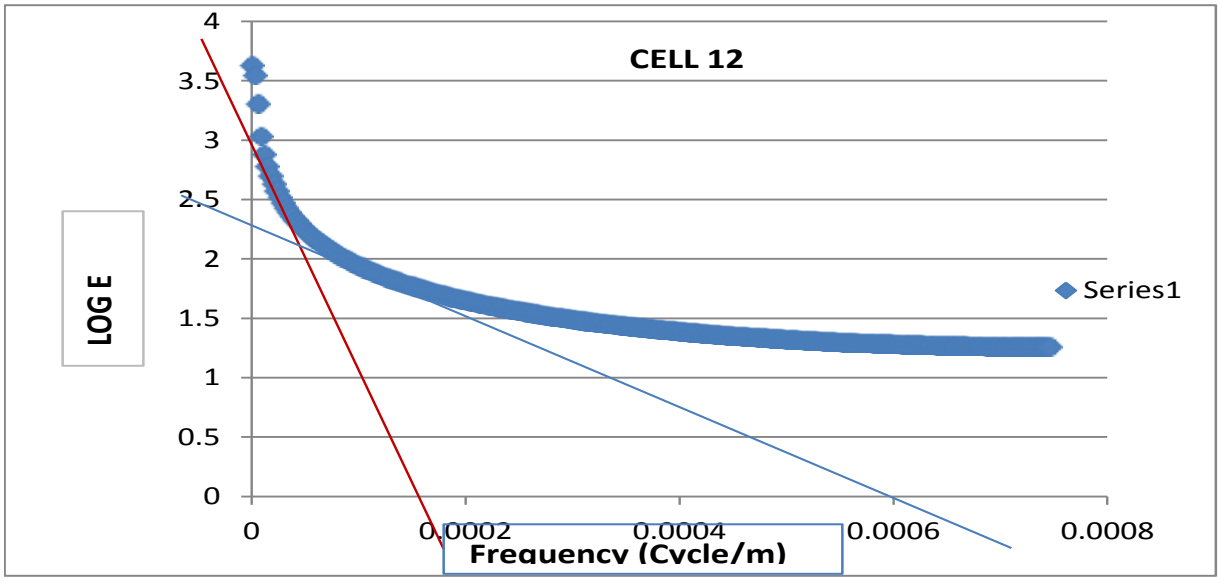
CELL 12
LOG E
Frequency (Cycle/m)
Series1
4
3.5
3
2.5
2
1.5
1
0.5
0
0
0.0002
0.0004
0.0006
0.0008

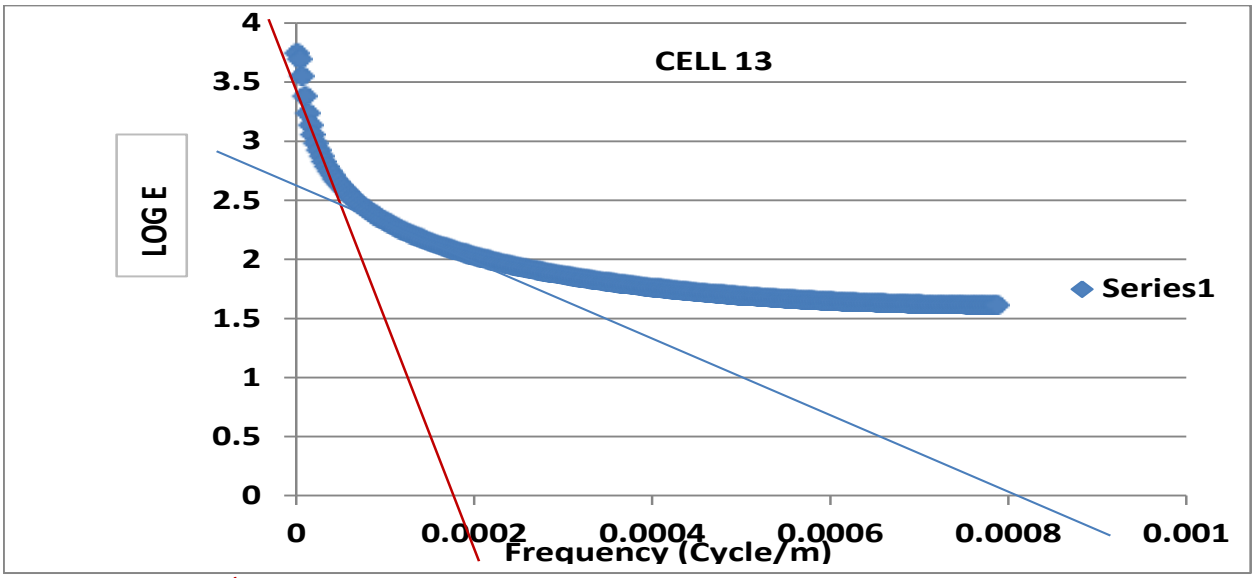
CELL 13
LOG E
Series1
4
3.5
3
2.5
2
1.5
1
0.5
0
0
0.0002
0.0004
0.0006
0.0008
0.001
Frequency (Cycle/m)

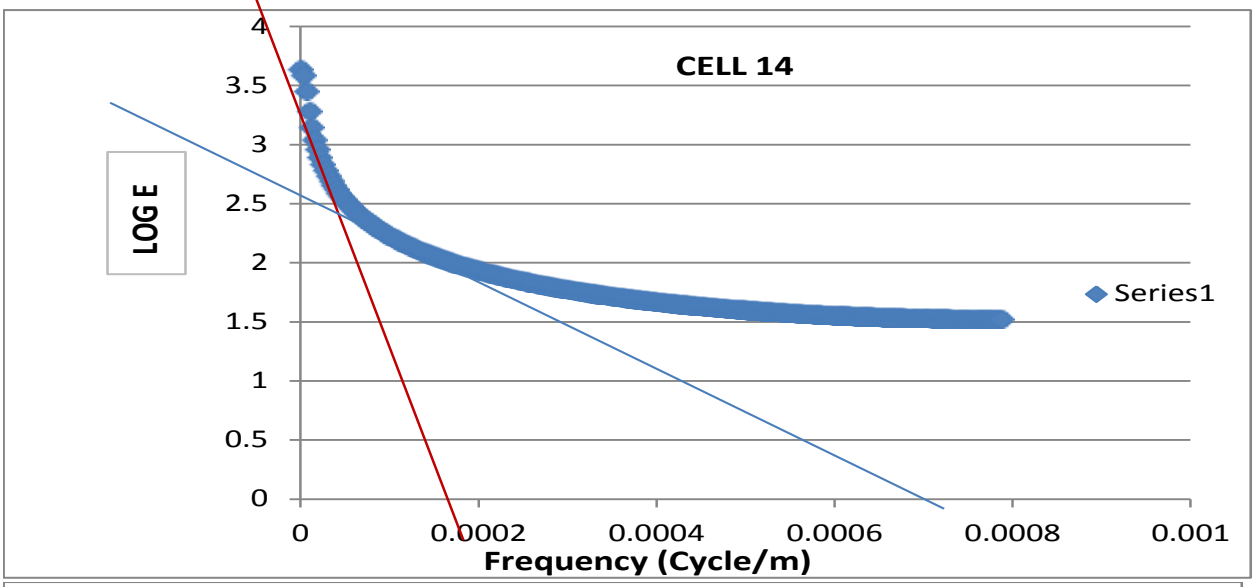
CELL 14
LOG E
Series1
4
3.5
3
2.5
2
1.5
1
0.5
0
0
0.0002
0.0004
0.0006
0.0008
0.001
Frequency (Cycle/m)

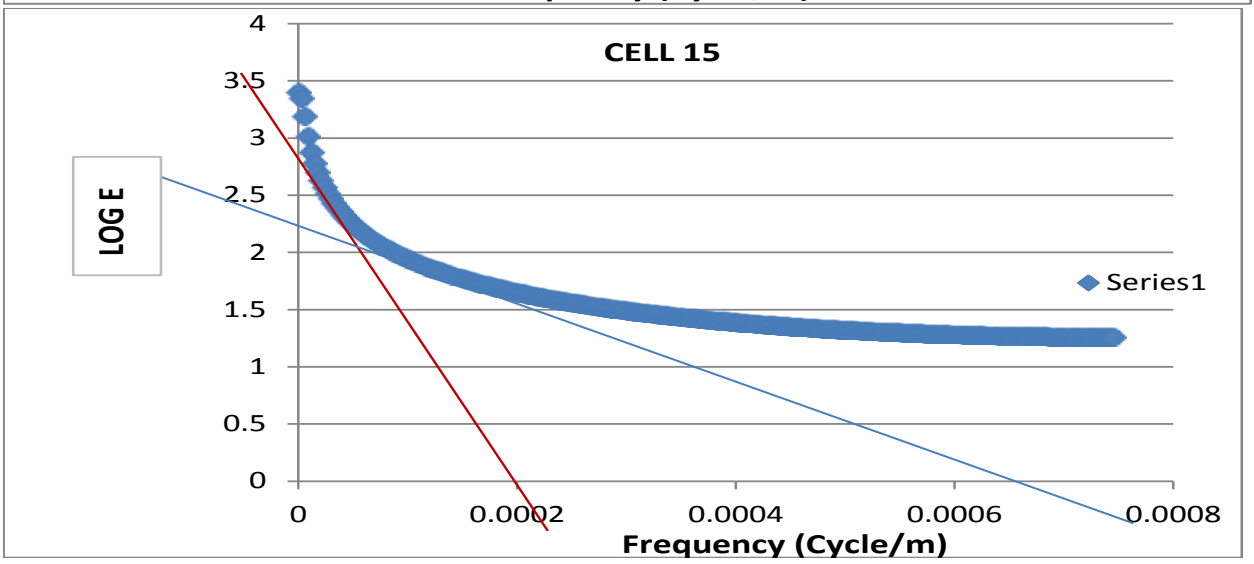
CELL 15
LOG E
Series1
4
3.5
3
2.5
2
1.5
1
0.5
0
0
0.0002
0.0004
0.0006
0.0008
Frequency (Cycle/m)

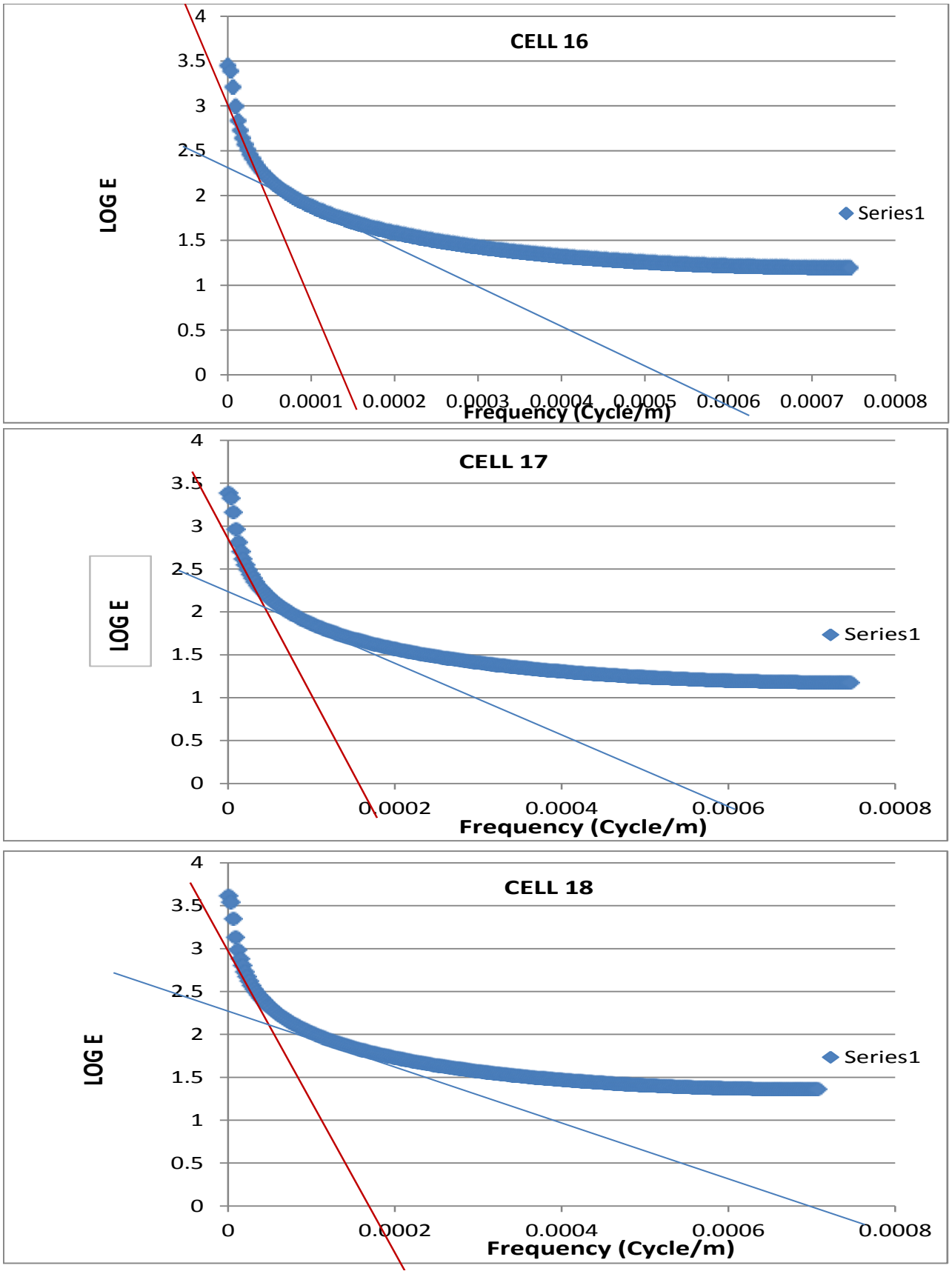

Figure 9. Spectral plots of log E against frequency of cells 1 to 18.

Table 1. Summary of the log E/frequency graphs for deep segments.

Cell number	Log E	Frequency (cycle/m)	Slope ($\Delta LogE/\Delta Freq$)	Deep depth (m)
1	2.9	0.00018	16111.11	2564.16
2	3.5	0.00015	23333.33	3713.62
3	3	0.0002	15000	2387.32
4	3.3333	0.00015	22222	3536.74
5	3.7	0.0001	37000	5888.73
6	3.25	0.00014	23214.29	3694.67
7	3	0.00015	20000	3183.10
8	2.5	0.0001	25000	3978.87
9	3.5	0.0001	35000	5570.42
10	1.75	0.00019	9210.53	1465.90
11	1	0.00008	12500	1989.44
12	3	0.00016	18750	2984.16
13	3.375	0.00017	19852.94	3159.69
14	3.25	0.00017	19117.65	3042.66
15	2.8	0.0002	14000	2228.17
16	3	0.00012	25000	3978.87
17	2.85	0.00017	16764.71	2668.19
18	3	0.00018	16666.67	2652.58
Average				3260.41

Table 2. Summary of the log E/frequency graphs for shallow segments.

Cell number	Log E	Frequency (rad/m)	Slope ($\Delta LogE/\Delta Freq$)	Shallow depth (m)
1	2.3333	0.00052	4487.115	714.15
2	2.75	0.0007	3928.571	625.25
3	2.5	0.0005	5000	795.77
4	2.5	0.0007	3571.429	568.41
5	3	0.0005	6000	954.93
6	2.5	0.0007	3571.429	568.41
7	2.125	0.0009	2361.111	375.78
8	1.625	0.0006	2708.333	431.04
9	2.6667	0.00054	4938.333	785.96
10	1.125	0.00057	1973.684	314.12
11	0.16667	0.000025	6666.8	1061.05
12	2.3	0.0006	3833.333	610.09
13	2.625	0.0008	3281.25	522.23
14	2.625	0.0007	3750	596.83
15	2.25	0.00065	3461.538	550.92
16	2.3	0.0005	4600	732.11
17	2.25	0.00054	4166.667	663.15
18	2.25	0.0007	3214.286	511.57
Average				632.32

of 3082 m using source parameter imaging (SPI) technique. However, the work of Igwesi and Umego (2013) who obtained two layer source model with depth for deeper magnetic source ranging from 1.16 km to 6.13 km with average depth value of 3.03 km and depth to shallower magnetic source ranging from 0.016 to 0.37 km with average depth value of 0.22 km fairly agrees with the result of the present work.

Table 3. Summary of spectral analysis result.

Cell No.	Median long. (m)	Median lat. (m)	Deeper depth (m)	Shallow depth (m)
1	287650	673450	2564.16	714.15
2	306150	673450	3713.62	625.25
3	324650	673450	2387.32	795.77
4	287650	691450	3536.74	568.41
5	306150	691950	5888.73	954.93
6	324650	691950	3694.67	568.41
7	288275.2	710450	3183.10	375.78
8	306275.2	710450	3978.87	431.04
9	324650	710450	5570.42	785.96
10	288400.4	728718.1	1465.90	314.12
11	306900.4	729218	1989.44	1061.05
12	328400.4	728718.1	2984.16	610.09
13	288400.4	746718.1	3159.69	522.23
14	306400.4	746718.1	3042.67	596.83
15	324900.4	746718.1	2228.17	550.92
16	288400.4	765218.1	3978.88	732.11
17	306400.4	765218.1	2668.19	663.14
18	324900.4	765218.1	2652.58	511.57
Average			3260.41	632.32

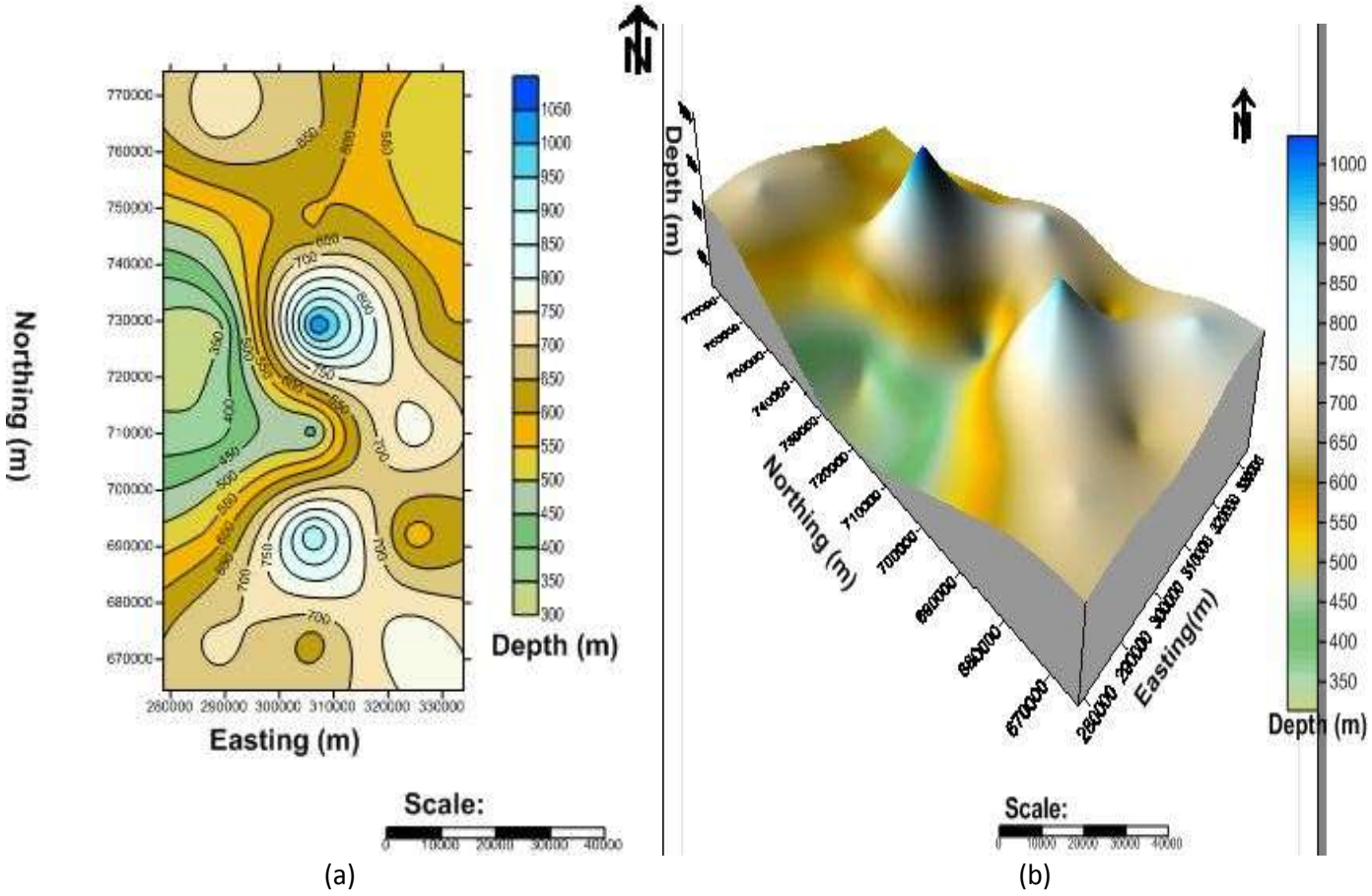

Figure 10. Map of (a) 2D and (b) 3D shallow depth of basement.

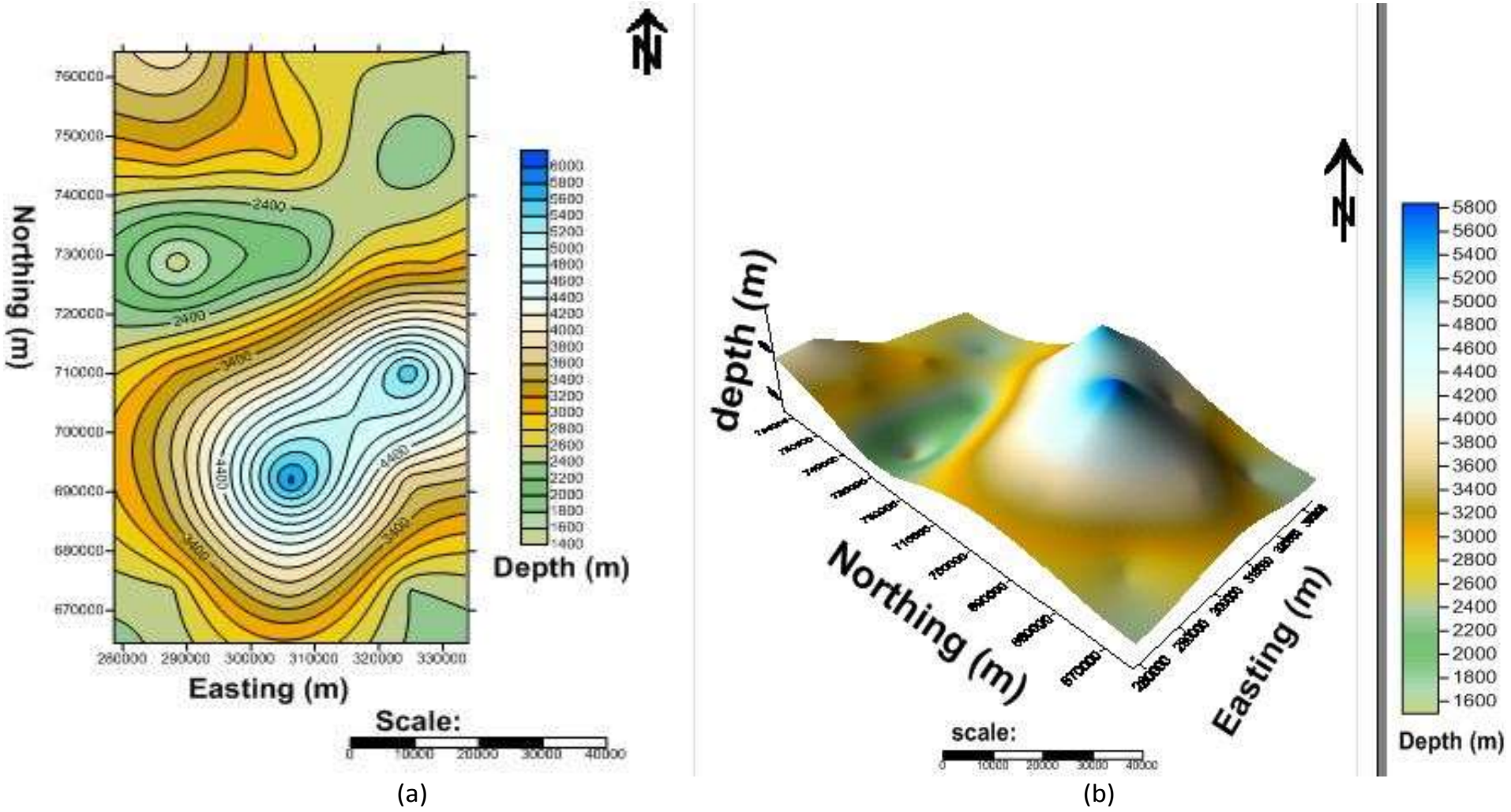

Figure 11. Map of (a) 2D and (b) 3D deep depth basement.

Conclusion

The interpretation of the aeromagnetic data of Nsukka and Udi areas was done qualitatively and quantitatively using spectral analysis approach. The Spectral Analysis has the shallow depth of 314.12 to 1061.05 m with average value of 632.32 m and deeper depth of 1465.90 to 5888.73 m with average value of 3260.41 m.

The result obtained was able to satisfy the objectives of this work, which includes the determination of depth to anomalous bodies or

determination of depth to basement of mineral causing the anomaly.

CONFLICT OF INTERESTS

The authors have not declared any conflict of interests.

REFERENCES

Aleke CG, Okogbue CO, Aghamelu OP, Nnaji NJ (2016). Hydrogeological potential and qualitative assessment of groundwater from the Ajali Sandstone at Ninth mile area, southeastern Nigeria. Environ. Earth Sci. 75:1-16.

Bhattacharyya BK (1966). Continuous spectrum of the total-magnetic-field anomaly due to a rectangular prismatic body. Geophysics 31(1):97-121.

Hahn A, Kind E, Mishra DC (1976). Depth estimate of magnetic sources by means of Fourier amplitude spectra. Geophy. Prosp. 24:287-308.

Hinze WJ, von Frese RRB, Saad AH (2013). Gravity and Magnetic Exploration. Cambridge University Press, Cambridge.

Igwesi ID, Umego NM (2013). Interpretation of aeromagnetic anomalies over some parts of lower Benue Trough using spectral analysis technique. Int. J. Sci. Technol. Res. 2(8):153–165.

Nwajide CS, Reijers TJA (1995). Sedimentology and sequence stratigraphy of selected outcrops in the upper cretaceous of lower Tertiary of the Anambra Basin. SPDC Exploration Report, XPMW 96007:21–37.

Nwankwo LI, Olasehinde PI, Akoshile CO (2011). Heat flow anomalies from the spectral analysis of airborne magnetic data of Nupe Basin, Nigeria. Asian J. Earth Sci. 2011:1-7

Obiora DN, Ossai MN, Okwoli E (2015). A case study of aeromagnetic data interpretation of Nsukka area, Enugu State, Nigeria, for hydrocarbon exploration. Int. J. Phys. Sci. 10(17):503-519.

Obiora DN, Ossai MN, Okeke FN, Oha AI (2016). Interpretation of airborne geophysical data of Nsukka area, southeastern Nigeria. J. Geol. Soc. India 88:654-667.

Onwuemesi AG (1995). Interpretation of magnetic anomalies from the Anambra Basin of southeastern Nigeria. Ph.D thesis, Nnamdi Azikiwe University, Awka, Nigeria.

Reeves C (2005). Aeromagnetic Surveys; Principles, Practice and Interpretation. GEOSOFT.

Shuey RT, Schellinger DK, Tripp AC, N1ey LB (1977). Curie depth determination from aeromagnetic spectra Geophys. J. R. Astr. Soc. 50:75-101.

Spector A, Grant FS (1970). Statistical models for interpreting aeromagnetic data. Geophysics 35:293-302.

Tadjou JM, Nouayou R, Kamguia J, Kande HL, Manguele-Dicoum E (2009). Gravity analysis of the boundary between the Congo Craton and the Pan-african belt of Cameroon. Aust. J. Earth Sci. 102:71-79.

Ugwuanyi MC, Ibuot JC, Obiora DN (2015). Hydrogeophysical study of aquifer characteristics in some parts of Nsukka and Igbo Eze south local government areas of Enugu State, Nigeria. Int. J. Phys. Sci. 10(15):425-435.